THE PHYSICAL PROPERTIES OF $(As_2Se_3)_{1-x}:Sn_x$ AND $(As_4S_3Se_3)_{1-x}:Sn_x$ GLASSES

O. V. Iaseniuc, D. V. Harea, E. E. Harea, G. F. Volodina, and M. S. Iovu

Institute of Applied Physics, Academy of Sciences of Moldova
Academiei str. 5, Chisinau, MD-2028 Republic of Moldova
E-mails: oxygena08@rambler.ru, dyanaharea@yahoo.com

(Received July 1, 2013)

Abstract

Experimental results on some physical and optical properties of $(As_2Se_3)_{1-x}:Sn_x$ and $(As_4S_3Se_3)_{1-x}:Sn_x$ (x = 0÷10 at %) glasses and amorphous films (d~2.0 μm) are presented. The bulk chalcogenide glasses are studied by *X*-ray diffraction spectroscopy and nanoindentation methods. It is established that the addition of these amounts of tin (x = 0÷10 at %) does not lead to significant changes in the physical properties of the glass, such as values of stress and Young's modulus related to the modification of the density and compactness. The XRD measurements show that the Sn impurities in the $(As_4S_3Se_3)_{1-x}:Sn_x$ do not significantly change the shape of the first sharp diffraction peak (FSDP) of the X-ray diffraction patterns either; the intensity and the position of the FSDP nonmonotonically depend on the Sn concentration. It has been found that the addition of these amounts of tin in $(As_4S_3Se_3)_{1-x}:Sn_x$ does not lead to significant changes in the glass physical properties, such as values of stress and Young's modulus related to the modification of the density and compactness. The study of the photoplastic effect is performed *in situ*, with illumination of the bulk and thin film samples during indentation as well as their indentation after illumination with a green laser (λ = 532 nm) at a power of P = 50 mV/cm^2. The hardness is calculated from load-displacement curves by the Oliver-Pharr method. A sharp increase in hardness is registered if the tin concentration exceeds a value of 3–4% Sn. The hardness H of $(As_2Se_3)_{1-x}:Sn_x$ films varies between 115 and 130 kg/mm^2. It is found that the hardness H of amorphous thin films is generally higher than the hardness of bulk samples with the same chemical composition. In this study, we are focused on the mechanical characteristics of high-purity $As_2Se_3:Sn_x$ thin films.

1. Introduction

Chalcogenide glasses (CGs), such as As_2S_3, As_2Se_3, As_2Te_3, As-S-Se, As-Sb-S(Se), As-Ge-S(Se), represent a new class of advanced materials exhibiting attractive combinations of properties, such as high strength/hardness and excellent wear/corrosion resistance [1–4], excellent optical properties (high refractive index, high transmittance in the near IR and IR regions of the spectrum), which make them good candidates for photonic and optoelectronic applications (optical elements and memories, optical sensors, nonlinear optical devices, holographic elements, IR telecommunications, biosensing, signal processing, and photonic applications [5–7]). The effect of light-induced photostructural transformations is characteristic of many amorphous chalcogenides films, and they have served as a base of many applications in photonics and optoelectronics, especially as inorganic photoresists for submicron technology [8, 9].

These distinguished properties are primarily due to a disordered atomic arrangement in the amorphous materials resulting in the absence of grain boundaries and defects in the microstructure. While the nonequilibrium nature of amorphous materials offers outstanding properties, it also presents significant challenges in the processing of these materials.

It is even more interesting to study the chalcogenides doped with metal impurities, which alter the physicochemical, electrical, and optical properties. It was shown that the Sn impurity introduced in the As_2Se_3, AsSe, and Sb_2S_3 glass network reduces the photodarkening effect [10–13]. Tin-containing chalcogenides showed the some deviation in behavior due to modification in the local ordering of the host chalcogenide matrix after the tin incorporation, which was observed in the bulk glasses as well as in the corresponding thin films.

For numerous applications, the mechanical behavior is one of important characteristics of the material [14–16]. Moreover, the photoplastical effect in some amorphous films (As-Se, Ss-S-Se) that occurs under band-gap illumination is described. This effect is considered electronic rather than thermal and consists of two parts: negative (decreasing in viscosity) and positive (increasing in viscosity); it occurs only under illumination. In the opinion of the authors, the first part of the photoplastic effect is general for CGs and causes all photostructural phenomena in amorphous materials.

The photoplastical effect is evident from the hardening of illuminated materials [17] as well as their softening [18]. The photoplastical effect depends on a number of factors, such as radiation power, temperature, and wavelength. Studies of the spectral dependence of photoplasticity showed a maximum effect under illumination of samples with a wavelength close to the band gap value [19]. Photoplasticity in chalcogenide films was studied in [20-22], where the effect was observed during illumination of samples with a wavelength comparable to the band gap value. The nature of the photoplastical effect remains poorly understood. The effect was attributed to thermal expansion of the film due to the absorption of exciting light as well as recombination of electrons and holes under photoexcitation. The properties of glass can be varied and regulated over an extensive range by modifying the composition and production techniques. It was shown that the addition of a tin impurity in amorphous As_2Se_3 films can provide a pronounced effect on electrical, transport properties, optical and photoinduced phenomena [23–27].

In this study, we have combined the experimental investigations of X-ray diffraction (XRD) measurements and the mechanical properties of bulk and thin films of $(As_2Se_3)_{1-x}$:Sn_x and $(As_4S_3Se_3)_{1-x}$:Sn_x (x = 0÷10 at % Sn) chalcogenides.

2. Experimental

The bulk CGs $(As_2Se_3)_{1-x}$:Sn_x and $(As_4S_3Se_3)_{1-x}$:Sn_x (x = 0÷10 at % Sn) glasses were prepared from the elements of 6N (As, S, Se, Sn) purity by a conventional melt quenching method. The starting components $As_4S_3Se_3$ and Sn were mixed in quartz ampoules and then evacuated to a pressure of P~10^{-5} torr, sealed and heated to a temperature of T = 900^{o}C at a rate of 1^{o}C/min. The quartz tubes were held at this temperature for 48 h for homogenization and then slowly quenched in a furnace. For nanoindentation and optical measurements of the bulk samples, planar parallel plates with a thickness of about d = 2÷3.5 mm were prepared and polished. Experiments were carried out at room temperature. Indentation was performed with CSM Indentation Testers (Ultra Nano, Nano and Micro; with max load P = 100 mN; load resolution of 0.001 μN) with software. Hardness (Hv) and Young's modulus (E) were

automatically computed. The X-ray diffraction (XRD) measurements were performed on a DRON-UM1 diffractometer using *Fe-Kα* radiation (λ = 1.93604 Å) with a Mn filter by the $\theta/2\theta$ scanning method. Thin film samples with a thickness of d = 0.5÷3 μm were prepared by vacuum flash thermal evaporation of the synthesized initial CG onto glass substrates held at T_{subs} = 100°C.

3. Results and Discussion

3.1. X-Ray diffraction measurements

Crystalline semiconductors are characterized by the ***ordering on distance***, e.g., by the existence of a correlation between two atoms situated at any distance in the network. The noncrystalline semiconductors preserve a ***short range order (SRO)*** in a range of 0.3-0.5 nm and are characterized by the existence of a correlation in the first atomic coordination sphere. In the case of dominantly covalently bounded amorphous solids, SRO is described by local coordination polygons, e.g., pyramidal AsS_3 in As_2S_3. In many amorphous semiconductors, such as CGs, this order is shown at longer distances, the so-called ***medium range order (MRO)*** which extends up to a range of 0.5-1.0 nm. For disordered semiconductors, a ***long range order (LRO)*** is absent, and this means that the amorphous chalcogenides have no translational symmetry.

The X-ray diffraction technique is a nondestructive method which gives information from the atomic scale range; it is a widely used method for investigations of disordered semiconductors with multilayered structures [28]. Using the X-Ray diffraction method, the diffraction patterns were obtained in the range of 2θ diffraction angles of 10° to 80° (θ is the Bragg angle) for CGs As_2S_3, As_2Se_3, $As_4S_3Se_3$, and $As_4S_3Se_3$:Sn_x (x = 0.01, 0.02, 0.04, 0.06, 0.07, and 0.10).

Figure 1 shows the angular distribution of X-Ray diffraction intensity for As_2S_3, As_2Se_3, and $As_4S_3Se_3$ chalcogenides glasses. The position of the first sharp diffraction peak (FSDP) for As_2S_3 is 2θ = 22.47° and increases to 2θ = 24.60° for As_2Se_3. For the intermediate composition of $As_4S_3Se_3$, the maximum of the FSDP is located at 2θ = 23.00°. These spectra represent a sum of diffraction patterns of is structural vitreous As_2S_3 and As_2Se_3 with three broad lines of diffractograms, which are similar to the unvelope of the rounded lines of the spectra of crystalline As_2S_3 and As_2Se_3. It can be assumed that, in the microcrystalline state of the investigated glasses, there are domains with an ordered structure with dimensions of about 15–20 Å. Previously, a analogy between the structure of vitreous and crystalline states of As_2S_3 was vindicated by short-range order investigations—interatomic distances and coordination numbers—with the addition of the radial distribution function [29].

It was established that Van der Waals forces with a reduced covalent component act between As_2S_3 and As_2Se_3 layers. The interaction forces between the layers are hundred times weaker than the binding forces between the layers. According to [28], the structure of the glasses represents an interlinking of As-S_3 and As-Se_3 pyramids that form rings with six units. The arsenic atoms are situated at the top of the pyramid, while the chalcogen atoms form the basis. As was shown, the crystalline semiconductors are characterized by a LRO; for example, there is a good correlation between the position of the each two atoms in the network, which is not found in noncrystalline semiconductors [30, 31]. Noncrystalline semiconductors exhibit only a SRO, which involves individual atoms in the first coordination sphere. Since the range order in CGs can be extended to several interatomic distances, a new concept of the average order was introduced (MRO).

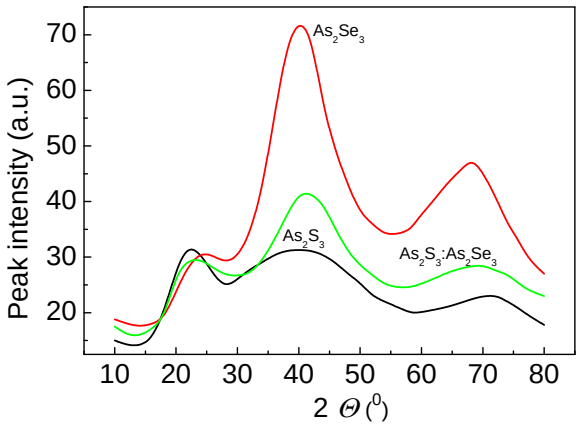

Fig. 1. X-ray diffraction patterns for As_2S_3, As_2Se_3, and $As_4S_3Se_3$ glasses.

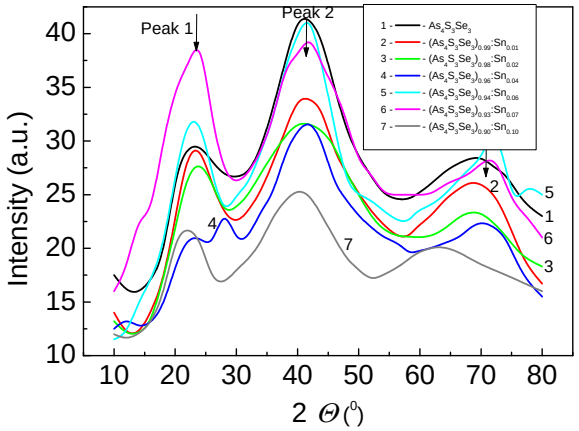

Fig. 2. X-ray diffraction patterns for $(As_4S_3Se_3)_{1-x}$:Sn_x glasses; *x*, at % Sn: (1) 0, (2) 1.0, (3) 2.0, (4) 4.0, (5) 6.0, (6) 7.0, and (7) 10.0.

Comprehensive studies of the FSDP of vitreous As_2S_3 and As_2Se_3 show that they have a similar structure [28]. According to [28], the first coordination spheres (first order neighbor position) of the central atom in the structure is r_1 = 2.414 Å for As_2Se_3, and r_1 = 2.306 Å for As_2S_3, respectively. The second coordination spheres (second order neighbor position) of the central atom in the structure is r_1 = 3.625 Å for As_2Se_3, and r_1 = 3.475 Å for As_2S_3, respectively.

The Sn concentration in the mixed glasses $As_4S_3Se_3$:Sn_x does not significantly change the shape of the FSDP of the X-ray diffraction patterns (Fig.2). In general, the diffraction patterns of the $As_4S_3Se_3$:Sn_x glasses are similar and form three wide lines, the maxima of which correspond to the interlayer distances d ~ 4.8 – 2.8 – 1.7 Å. As in the case of As_2Se_3:Sn_x [31], the angular position of the FSDP in $As_4S_3Se_3$:Sn_x slightly depends on the Sn concentration. Figures 3 and 4 show the angular position and the intensity of the FSDP in the X-ray diffraction patterns of As_2S_3 (1), As_2Se_3 (2), and $As_4S_3Se_3$ (3), and the FSDP in the X-ray diffraction patterns of the $(As_4S_3Se_3)_{1-x}$:Sn_x glasses.

Some parameters of the X-ray diffraction patterns of the investigated CGs are listed in Table 1. Figures 5 and 6 show the dependences of the peaks intensities vs. concentrations of tin of the three diffraction peaks of CG $As_4S_3Se_3$:Sn_x situated at 2θ~22.86÷23.67°, 2θ~40.34÷42°, and 2θ~62÷70°, and the dependence of the angular position of the diffraction peaks vs. tin concentration, respectively. The intensity of the FDSP shows a nonlinear behavior with the different amounts of doping with Sn. The maximum intensity is achieved at about 6 at % Sn in $As_4S_3Se_3$:Sn_x, while in the case of As_2Se_3:Sn_x the maximum intensity is situated at the tin concentration of about 2 at % Sn. A similar behavior was found for the second and third diffraction peaks. According to [31], when Sn is added in As_2Se_3 or As_2S_3 ChGs, due to the tetrahedral disposal of the sp3 bonds in the chalcogens, the dopant atom implanted in the network increases the thickness of the layered configuration as revealed by a significant shift of the FSDP towards lower angles. This implantation corresponds to the introduction of the structural units of the $SnSe_2$ or SnS_2 type in the glass network; the same fact was confirmed by the Mössbauer spectroscopy experiments [11].

Table 1. Parameters of the X-ray diffraction patterns of the studied As_2S_3, As_2Se_3, and $(As_4S_3Se_3)_{1-x}$:Sn_x CGs

N/o	Glass composition	Position of Peak 1, 2θ	Intensity of Peak 1, a.u.	Position of Peak 2, 2θ	Intensity of Peak 2, a.u.	Position of Peak 3, 2θ	Intensity of Peak 3, a.u.
1	As_2S_3	22.32	31.36	40.50	31.07	71.78	22.92
2	As_2Se_3	24.35	30.52	40.50	71.54	68.25	46.81
3	$As_4S_3Se_3$	22.86	29.43	41.01	41.14	69.28	28.37
4	$(As_4S_3Se_3)_{0.99}$:$Sn_{0.01}$	23.39	29.06	41.53	33.92	69.15	26.09
5	$(As_4S_3Se_3)_{0.98}$:$Sn_{0.02}$	23.67	27.54	41.14	31.64	68.61	23.51
6	$(As_4S_3Se_3)_{0.96}$:$Sn_{0.04}$	22.86	20.93	41.53	31.49	70.62	22.38
7	$(As_4S_3Se_3)_{0.94}$:$Sn_{0.06}$	23.00	31.64	41.53	41.14	72.08	30.35
8	$(As_4S_3Se_3)_{0.93}$:$Sn_{0.07}$	23.39	38.33	41.81	39.17	71.55	28.15
9	$(As_4S_3Se_3)_{0.90}$:$Sn_{0.10}$	21.93	21.69	40.34	25.26	62.75	20.17

*) *For the $(As_4S_3Se_3)_{0.96}$:$Sn_{0.04}$ glass composition, an additional peak at 2θ = 28.20 was observed.*

3.2. Physical properties and photoplastic effect in As_2Se_3:Sn_x glasses

The physical properties (density, hardness, glass transition temperature, electrical conductivity, etc.) of amorfous As-Se films have been previously reviewed by Borisova [32, 33]. The investigation of bulk, thin films, and illuminated thin film samples was performed using a NHT CSM nanohardnes tester. The hardness was calculated from load-displacement curves by the Oliver-Pharr method. *In-situ* illumination of samples was carried with a green laser (λ = 532 nm) with a power of P = 50 mV/cm^2. To change the direction of the incident laser beam, an optical glass prism was used (Fig. 7).

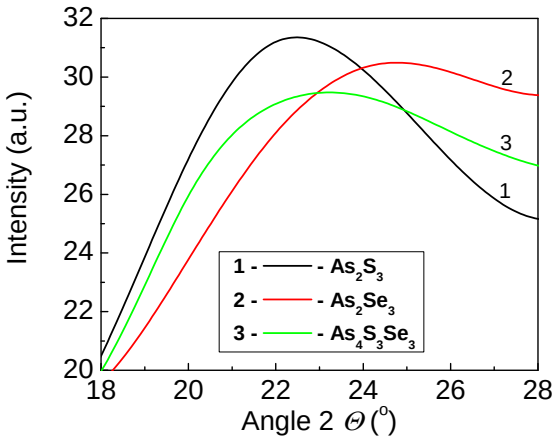

Fig. 3. FSDP in the X-ray diffraction patterns of As_2S_3 (1), As_2Se_3 (2), and $As_4S_3Se_3$ (3).

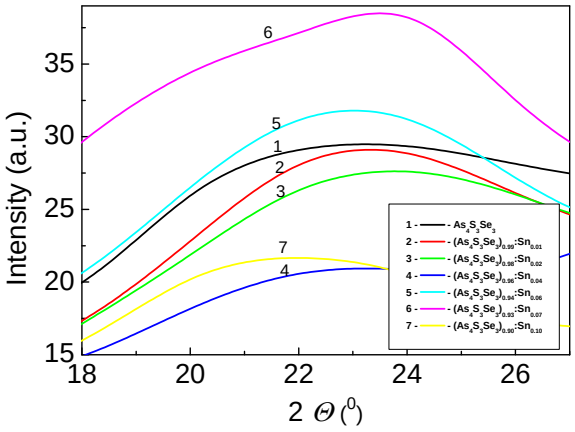

Fig. 4. FSDP in the X-ray diffraction patterns of $(As_4S_3Se_3)_{1-x}$:Sn_x; x, at % Sn: (1) 0, (2) 1.0, (3) 2.0, (4) 4.0, (5) 6.0, (6) 7.0, and (7) 10.0.

The maximum indentation load was 5 mN; therefore, the maximal penetration depth did not exceed 15% of the film thickness. The hardness was calculated using the expression

$$H_B = (1570 * P) / l^2, \quad (1)$$

where P is the applied load and L is the height of the triangle of the remaining imprints [34]. For both the bulk samples and the amorphous thin films, the applied load was 10 g and the depth of deposited imprints did not exceed 20% of the films thickness.

Figure 8 shows variations in glass transition temperature $T_g(x)$ for the bulk $As_2Se_3:Sn_x$ glasses and the nonreversing heat $\Delta H_{nr}(x)$. At low concentrations of the Sn additive, the glass transition temperature T_g of the base glass increases with x, suggesting that the base glass becomes more bound. However, as x approaches 5 at % Sn, the glass transition temperature T_g exhibits a threshold behavior [11].

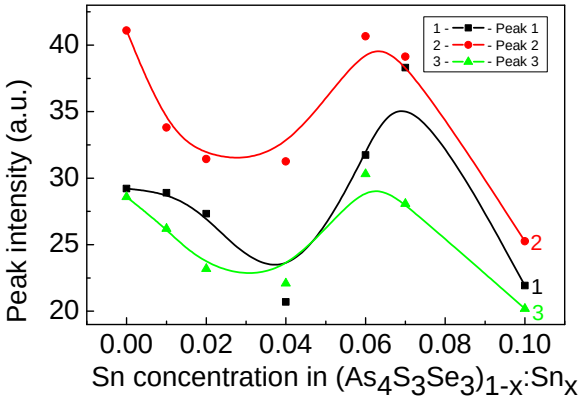

Fig. 5. Dependence of the angular position of the diffraction peaks vs. concentration of tin in some $As_4S_3Se_3:Sn_x$ CGs.

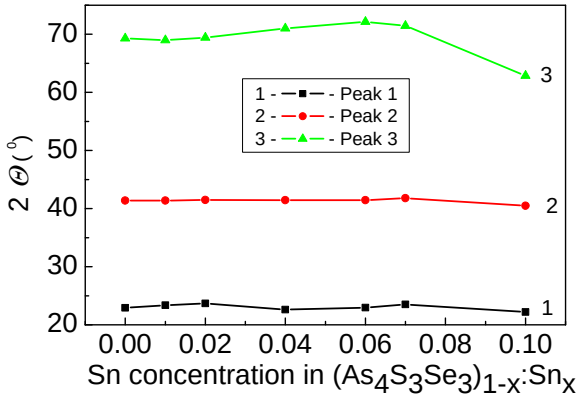

Fig. 6. Dependence of the angular position of the diffraction peaks vs. concentration of tin in the some $As_4S_3Se_3:Sn_x$ CGs.

The maximum in T_g suggests [11, 24] that the above threshold additives no longer form part of the base glass structure, e.g., they undergo nanoscale phase separation. These nanoscale phase separation effects have already been found in As_2Se_3 base glass ($x = 0$) and are apparently attributed to higher concentrations of Sn (x > 5 at % Sn). Mössbauer spectroscopy results show the presence of a single line (A) feature in the spectra at low x (<3 at %). The isomer-shift of this line has been previously assigned [35] to Sn that is tetrahedrally coordinated to 4 Se near-neighbors as in a $Sn(Se_{1/2})_4$ local structure [11]. Apparently, the introduction of a Sn additive in As_2Se_3 base glass contributes to the growth of $Sn(Se_{1/2})_4$ units and makes the base glass As-rich. The effect can occur in one of two modes: through the formation of either polymeric ethylene-like $As_{2(}Se_{1/2})_4$ units and/or monomeric As_4Se_4 cages based on the Realgar structure. It is found that, in the base glass, the polymeric species are first nucleated at x slightly below 0.4, and monomeric ones are formed afterwards (x > 0.42).

The experimental results of investigation of hardness for bulk and $As_2Se_3:Sn_x$ amorphous thin films are presented in Figs. 9 and 10 and are in good agreement with experimental results obtained earlier by Borisova [32, 33]. The hardness values of bulk samples depend on the Sn

concentration in the As_2Se_3:Sn_x glasses and vary between 1300 and 1700 MPa.

The hardness H of the amorphous As_2Se_3:Sn_x thin films exhibits a nonmonotonic behavior in dependence on the Sn concentration and is higher than the hardness of bulk samples. An increase in hardness is registered at an impurity concentration of about 4% Sn. The hardness H of $(As_2Se_3)_{1-x}$:Sn_x films varies between 1730÷1780 MPa. For both bulk samples and thin films, the hardness is higher according to the data obtained in [32, 33]. This fact can be attributed to some technological features in preparing the ChG. Under illumination, the hardness H of $(As_2Se_3)_{1-x}$:Sn_x decreases, and this decrease is specific especially of the doped samples (Fig. 10).

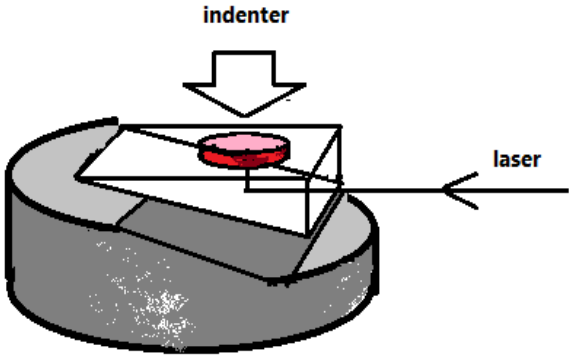

Fig. 7. Experimental set-up for investigation of the photoplastical effect in CGs.

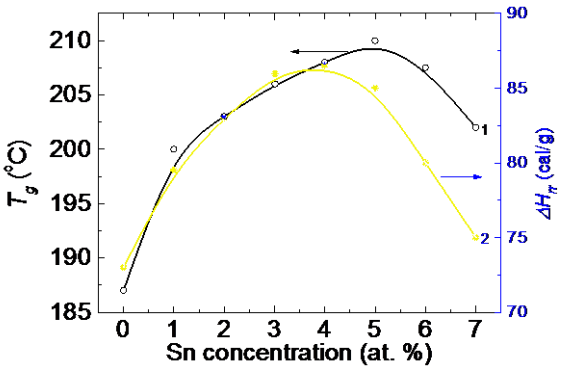

Fig. 8. Variations in $T_g(x)$ (1), $\Delta H_{nr}(x)$ for As_2Se_3:Sn_x glasses. The smooth lines are computer fitting.

For investigation of microhardness and Young's modulus, a Nano-Indentation Tester (NIT) was used; it provides experimental data by indenting to depths at a nanometer–micron scale. This nanoindenter can be used to characterize organic, inorganic, soft or hard materials, and coatings. The mechanical characterization of the surface of bulk materials can also be performed, including metals, semiconductors, glasses, composites, and in vitro biomaterials.

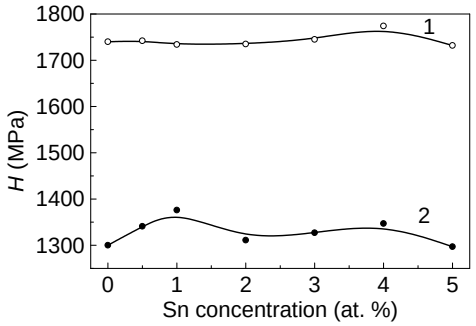

Fig. 9. Hardness H of $(As_2Se_3)_{1-x}$:Sn_x. samples, thin films (1) and bulk (2).

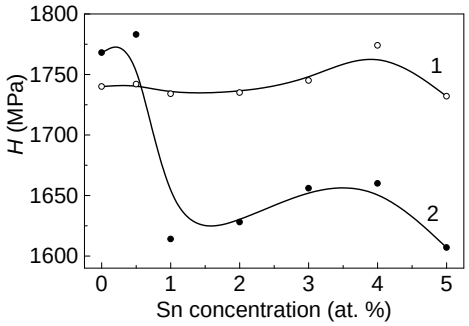

Fig. 10. Hardness H of $(As_2Se_3)_{1-x}$:Sn_x as-deposited (1) and illuminated (2) thin films.

The operating principle of the tester is as follows: an indenter diamond tip, normal to the

sample surface, is driven into the sample by applying an increasing load (P = 100 mN) up to a certain preset value. The load is then gradually decreased until partial or complete relaxation of the material occurs. After the removal of the load, the diagonal length is measured (imprint d_1 and d_2). The offset of diagonal tip was < 0.25 μm and the load resolution was 0.001 N. To avoid overlapping of surface stresses developed around neighboring indentations, the separation between indentation diagonals was kept more than ten times the diagonal length of indentation impressions.

The dimensions of both diagonals d made at a particular load P were measured, and the average diagonal d was calculated [14]. The value of microhardness H_V was computed from the $P(d)$ data using the standard well-known relation:

$$H_V = \frac{kP}{d_2}, \tag{2}$$

where k is the geometrical conversion factor for the indenter used (k = 0.1891):

$$k = \frac{1}{g}\left(2\sin\frac{136^0}{2}\right), \tag{3}$$

where g is the acceleration of gravity, 136º is the angle between its opposite faces of pyramidal tip. The average values of indentation diagonal d and microhardness H_V for at least 10 indentations were used in the analysis of indentation size effect and hardness measurements.

Figure 11 shows the Young's modulus and microhardness dependences for the bulk samples of As_2S_3, As_2Se_3, and for $(As_4S_3Se_3)_{1-x}$:Sn_x (x = 0 ÷ 10 at %) vs tin concentration. It was observed that the addition of tin in the host material initially leads to an increase in the microhardness up to 2.0 at % Sn. A further increase in the Sn concentration decreases the microharness.

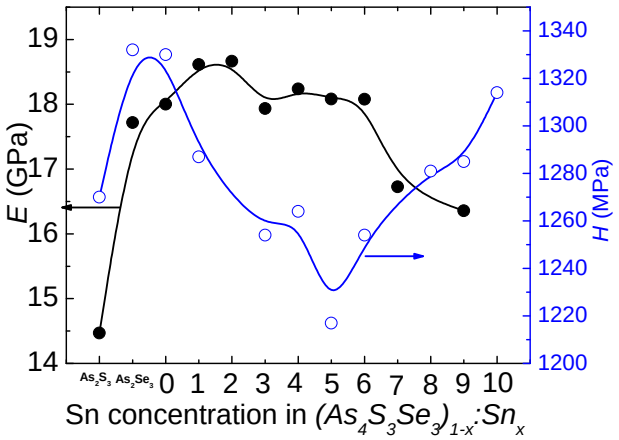

Fig. 11. Concentration dependence of Young's modulus E and microhardness H of the bulk samples As_2S_3, As_2Se_3, and $(As_4S_3Se_3)_{1-x}$:Sn_x.

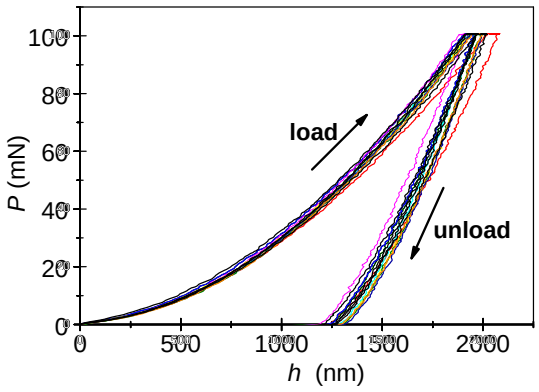

Fig. 12. Depth dependence of the load and unload values on chalcogenide samples of $(As_4S_3Se_3)_{1-x}$:Sn_x.

In general, the hardness varies around one value H_{middle} = 1282 MPa. A similar behavior was observed for the system $(As_2S_3)_{1-x}$:$(Sb_2S_3)_x$, where a curve with the minimum at about 2–3 at % of (Sb_2S_3) was obtained [36]. At the same time, the value of microhardness for vitreous

As_2S_3 and As_2Se_3 better coincides with the values cited in [37], although the Young's modulus in our case is higher by an order. According to [36], the observed increase in the hardness with x in the $(As_2S_3)_{1-x}$:$(Sb_2S_3)_x$ system indicates structural changes, which lead to lower molecular or configuration mobility.

Figure 12 represents the depth dependence of the load and unload values for chalcogenide samples of $(As_4S_3Se_3)_{1-x}$:Sn_x. Similar dependences were obtained for amorphous As_2S_3 thin films prepared by thermal deposition in vacuum [38]. The author mentions this fact in these experiments because the hold segment is rather long and the unloading process is very fast, any further viscoplastic creep during unloading is negligible compared to the elastic recovery during the unloading procedure. Figure 4 represent the imprint on the surface of the diamond tip on a $(As_4S_3Se_3)_{1-x}$:Sn_x sample at a load of P = 100 mN.

Figure 13 shows the surface morphology of the as-deposited amorphous $(As_2Se_3)_{0.90}$:$Sn_{0.10}$ thin film under the indentation load after (a) and before light illumination (b, upper patterns). For comparison, at the bottom of the figure, the pictures of the light-induced anisotropic plasticity in amorphous $As_{20}Se_{80}$ thin films are shown: (a) the image of the nonirradiated film surface and (b) the image of this surface by irradiated linearly polarized laser beam (λ = 633 nm) [39]. In both cases, after light irradiation, the plasticity of the investigated amorphous films increases. For explanation of this phenomenon, the authors of [38] proposed a mechanical model of anisotropic plasticity in CGs, according to which the anisotropic softening consists in the weakening of mechanical compliance in the orthogonal direction to the light polarization.

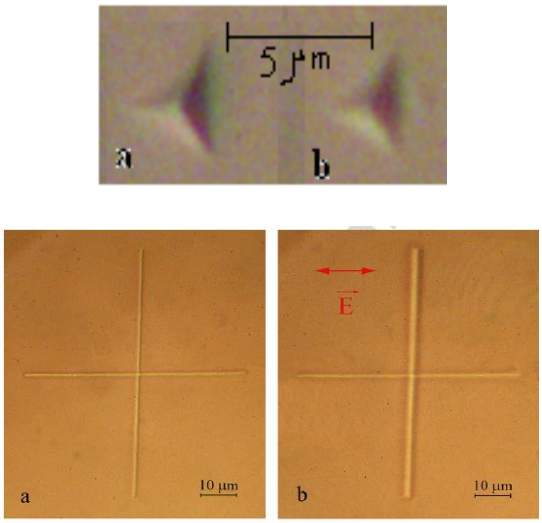

Fig. 13. Surface morphology of the as-deposited amorphous $(As_2Se_3)_{0.90}$:$Sn_{0.10}$ thin film under indentation load after (a) and before light illumination (b, upper patterns).

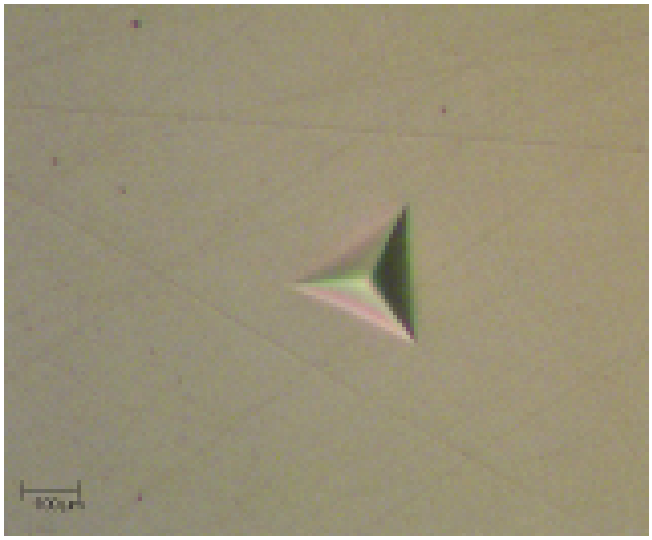

Fig. 14. Example of imprint on the surface of the diamond tip on bulk $(As_4S_3Se_3)_{1-x}$:Sn_x samples at a load of P = 100 mN.

4. Conclusions

The bulk of $(As_4S_3Se_3)_{1-x}$:Sn_x (x = 0÷10 at % Sn) CGs have been investigated by X-ray diffraction and nanoindentation methods. It has been found that the addition of these amounts of tin does not lead to significant changes in the glass physical properties, such as values of stress

and Young's modulus related to the modification of the density and compactness. The additions of Sn atoms in the CG matrix considerably decrease the elasticity of this material or increase the hardness at some tin concentrations. The XRD measurements have shown that the Sn impurities in the $(As_4S_3Se_3)_{1-x}$:Sn_x do not significantly change the shape of the FSDP of the X-ray diffraction patterns either; the intensity and the position of the FSDP nonmonotonically depend on the Sn concentration. The addition of As_2Se_3 in As_2S_3 shifts the FSDP towards higher diffraction angles from $2\theta = 22.47^o$ for As_2S_3 up to $2\theta = 24.60^o$ for As_2Se_3. The FSDP intensity increases at about 5.0–7.0 at % Sn in the $(As_4S_3Se_3)_{1-x}$:Sn_x glasses.

It has been found that the addition of these amounts of tin in $(As_4S_3Se_3)_{1-x}$:Sn_x does not lead to significant changes in the glass physical properties, such as values of stress and Young's modulus related to the modification of the density and compactness. The study of the photoplastic effect has been performed *in situ*, with illumination of the bulk and thin film samples during indentation as well as their indentation after illumination with a green laser (λ = 532 nm) at a power of $P = 50$ mV/cm^2. The hardness is calculated from load-displacement curves by the Oliver-Pharr method. A sharp increase in hardness is registered if the tin concentration exceeds a value of 3–4% Sn. The hardness H of $(As_2Se_3)_{1-x}$:Sn_x films varies between 115 and 130 kg/mm^2. It has been found that the hardness H of amorphous thin films is generally higher than the hardness of bulk samples with the same chemical composition.

Acknowledgments. The work was supported by the national project no. 11.817.05.03A.

References

[1] A. Inoue, B. Shen, and N. Nishiyama, Eds. M. Miller, P. Liaw, Springer, 2008, pp. 1–25.
[2] A. Inoue, B. Shen, and A. Takeuchi, Mater. Trans. 47, 1275 (2008).
[3] A. Inoue, Mater. Sci. Eng. A, 304–306, 1, (2009).
[4] W. L. Johnson, MRS Bull., 24, 42, (1999).
[5] A. Zakery and S. R. Elliot, Springer, Berlin-Heidelberg-New York, 2007.
[6] A. M. Andriesh, M. S. Iovu, and S. D. Shutov, J. Optoel. Adv. Mater. 4(3), 631 (2002).
[7] P. Nemec, J. Jedelsky, M. Frumar, M. Štábl, and M. Vlček, J. Phys. Chem. Solids, 65(7), 1253 (2004).
[8] A. Gerbreders and J. Teteris, J. Optoel. Adv. Mater. 9(10), 3164 (2007).
[9] M. Reinfelde and J. Teteris, J. Optoel. Adv. Mater. 13(11-12), 1531 (2011).
[10] M. Iovu, S. Shutov, and M. Popescu, J. NonCryst. Solids, 924 (2002).
[11] P. Boolchand, D. Georgiev, and M. Iovu, Chalcogenide Letters 2(4), 27 (2005).
[12] M. Iovu, P. Boolchand, and D. Georgiev, J. Optoel. Adv. Mater. 7(2), 763 (2005).
[13] M. Iovu, D. Harea, and E. Colomeico, J. Optoel. Adv. Mater. 10(4), 862 (2008).
[14] Lim Yong Yee and M.Munawar Chaudhri, Mech. Mater. 38, 1213 (2006).
[15] M. L. Trunov and V. S. Bilanich, J. Optoel. Adv. Mater. 5(5), 1085 (2003).
[16] S. N. Yannopoulos and M. L. Trunov, Phys. Status Solidi B 246(8), 1773 (2009).
[17] Yu. A. Osipyan and I. B. Savchenko, Pis'ma Zh. Eksp. Teor. Fiz. **7**, 130 (1968);
[18] A. B. Gerasimov, G. D. Chiradze, and N.G. Kutivadze, Semiconductors, 35, 72 (2001).
[19] L. Carlsson and C. Svensson, J. Appl. Phys. 41, 1652 (1970);
[20] A. Matsuda, H. Mizuno, T. Takayama, M. Saito, and M. Ki-kuchi, Appl. Phys. Lett. 25, 411 (1974).
[21] T. Igo, Y. Noguchi, and H. Nagai, Appl. Phys. Lett. 25, 193 (1974).
[22] H. Koseki and A. Odajima, Jpn. J. Appl. Phys. 21, 424 (1982).

[23] M. S. Iovu, S. D. Shutov, and L. Toth, Physica Status Solidi (b), 195, 149 (1996).
[24] M. S. Iovu, N. N. Syrbu, S. D. Shutov, I. A. Vasiliev, S. Rebeja, E. Colomeico, M. Popescu, and F. Sava, Physica Status Solidi (a), 175(2), 623 (1999).
[25] M. S. Iovu, S. D. Shutov, V. I. Arkhipov, and G. J. Adriaenssens, J. Noncryst. Solids 299&302, 1008 (2002).
[26] P. Boolchand, D. G. Georgiev, and M. S. Iovu, Chalcogenide Lett. 2(4), 27 (2005).
[27] M. S. Iovu, D. V. Harea, I. A. Cojocaru, E. P. Colomeico, A. Prisacari, and V. G. Ciorba, J. Optoel. Adv. Mater. 9(10), 3138 (2007).
[28] M. Popescu, A. Andries, V. Ciumas, M. Iovu, S. Sutov, and D. Tiuleanu, Fizica sticlelor calcogenice, Editura Stiintifica Bucuresti – I.E.P., Stiinta, Chisinau, 1996.
[29]. L. Tatarinova, The structure of amorphous solids and liquids, Nauka, Moscow, 151, 1983.
[30] M. Popescu, In: Physics and Applications of Noncrystalline Semiconductors in Optoelectronics, Eds. A. Andriesh and M. Bertolotti, 36, 215 (1996).
[31] M. Popescu, F. Tudorica, A. Andriesh, M. Iovu, S. Shutov, M. Bulgaru, E. Colomeyko, S. Malkov, V. Verlan, M. Leonovici, V. Mihai, and M. Steflea, Buletinul Academiei de Stiinte a Republicii Moldova, Fizica si tehnica 3, 3 (1995).
[32] Z. U. Borisova, Glassy Semiconductors (Plenum Press, New Yok, 1981) pp. 215–220 and references therein.
[33] Z. U. Borisova, , Chalcogenide semiconducting glasses, Khimiya, St. Petersburg, 1983 (in Russian).
[34] Yu. S. Boyarskaya, Physics of microindentitation processes, Stiinta, Kishinev, 1986 (in Russian).
[35] P. Kumar and R. Thangaraj, J. Noncrystalline Solids 352, 2288 (2006).
[36] F. Sava, J. Optoel. Adv. Mater. 3(2), 425 (2001).
[37] N. N. Shchurova and N. D. Savchenko, J. Optoel. Adv. Mater. 3(2), 491 (2001).
[38] M. L. Trunov, J. Phys. D: Appl. Phys. 41, 074011 (9pp), 2008.
[39] S. N. Yannopoulos and M. L. Trunov, Phys. Status Solidi, B 246 (8), 1773 (2009).